crystals

MDPI

Article

Ca-induced Plasticity in Magnesium Alloy: EBSD Measurements and VPSC Calculations

Umer Masood Chaudry, Kotiba Hamad * and Jung-Gu Kim *

School of Advanced Materials Science & Engineering, Sungkyunkwan University, Suwon 16419, Korea; umer@skku.edu

* Correspondence: hamad82@skku.edu (K.H.); kimjg@skku.ac.kr (J.-G.K.)

Received: 3 January 2020; Accepted: 23 January 2020; Published: 24 January 2020

Abstract: In the present work, Ca-induced plasticity of AZ31 magnesium alloy was studied using electron backscattered diffraction (EBSD) measurements supported by viscoplastic self-consistent (VPSC) calculations. For this purpose, alloy samples were stretched to various strains (5%, 10%, and 15%) at room temperature and a strain rate of 10^{-3} s^{-1}. The EBSD measurements showed a higher activity of non-basal slip system (prismatic slip) as compared to that of tension twins. The VPSC confirmed the EBSD results, where it was found that the critical resolved shear stress of the various slip systems and their corresponding activities changed during the stretching of the alloy samples.

Keywords: AZ31-Ca magnesium alloy; plasticity; slip systems; EBSD; VPSC; microstructure; texture

1. Introduction

Due to its low density and high natural abundance, magnesium (Mg) is considered as one of the most promising metals for structural applications. On the other hand, the naturally intrinsic brittleness of Mg, which is related to the hexagonal close packed (HCP) structure, limits its applicability as a structural material. In such structures, various slip families with several slip systems are usually available; those families are basal, prismatic, and pyramidal [1,2]. In spite of the presence of various slip families, the number of independent slip systems that can operate at room temperature are limited to those only belonging to the basal family, and this is due to the high critical resolved shear stress (CRSS) of prismatic and pyramidal slip systems (~40 and ~100 times higher than that of basal systems) [3]. One way to enhance the poor ductility of Mg-based materials is by weakening the basal texture observed after a primary processing (casting and rolling, for example). The evolution of weak texture leads to a higher activation of the non-basal systems due to the higher shear stress that can be resolved in the slip plane. Texture weakening in Mg alloys can be achieved through a thermomechanical processing of these alloys. For example, a weak basal-textured AZ31 alloy has been fabricated using a warm severe plastic deformation through differential speed rolling (DSR) process [4,5]. The results showed that the processing by DSR could optimize both strength and ductility in AZ31 Mg alloy, and this was related to the role of DSR in grain refinement and texture weakening of the AZ31 alloy. In addition, intermetallic compounds (IMC) formed due to the alloying of Mg with other elements can improve the ductility of Mg-based materials, where these compounds have a dual effect on the ductility. One is that these IMCs can contribute to the texture weakening during the primary processing, and hence, improve the ductility [6,7]. Another effect comes from the role of IMCs in changing the activity of the various slip systems, and this is related to the strengthening effect of the IMC in the basal plane [2,8]. Very recently, it has been reported that addition of 0.5wt. % calcium (Ca) can efficiently enhance the ductility and stretch formability of AZ31 Mg alloy [8], and this was attributed to the texture weakening induced by the $(Mg,Al)_2Ca$ particles. Viscoplastic self-consistent (VPSC) calculations conducted on sample strained to 10% showed that the Ca addition can change the

activity of the various slip systems. To gain further understanding of the Ca-induced plasticity in the AZ31 Mg alloy, more experiments and investigations are needed. Hence, the present study investigates the microstructural, textural evolution and deformation mechanisms of AZ31-0.5Ca as a result of various stretching conditions. In addition, particular focus was given to the slip behaviors and their related activities at various loading conditions. Accordingly, in the present work, VPSC calculations will be conducted on samples strained at various conditions, and these calculations will be supported by electron-back scattered diffraction (EBSD) measurements.

2. Experiments and VPSC Procedure

The composition of AZ31-0.5Ca Mg alloy investigated in the present work was 3.12 wt. % Al, 0.76 wt. % Zn, 0.5 wt. % Ca, 0.3 wt. % Mn and the balance is Mg. Samples (120 mm × 40 mm) cut from the alloy were stretched at room temperature and a strain rate of 10^{-3} s^{-1}. For EBSD measurements, specimens cut from the TD-RD (direction-rolling direction) plane of the stretched alloy samples were mechanically ground and polished using a cross-sectional polisher. The EBSD data were analyzed by using TSL OIM 6.1.3 software (EDAX Corporate, New Jersey, NY, USA). Electron probe micro-analyzing (EPMA) was also carried out on the non-stretched alloy.

To identify the deformation modes, which might be activated during the pre-stretching experiment, plasticity simulations based on a viscoplastic self-consistent (VPSC) model with full constraints (FC) approach were performed. The FC approach was used to account for the average overall response of the grains as a result of deformation. It is already established that a VPSC model can successfully predict the relative activities of various slip systems by comparing the simulated texture to the experimentally received texture based on the Voce hardening equation [9,10].

$$\tau^s = \tau_0^s + \left(\tau_1^s + \theta_1^s G\right)\left(1 - \exp\left(-G\left|\frac{\theta_0^s}{\tau_1^s}\right|\right)\right) \quad (1)$$

where Γ is accumulated shear strain and s, $\theta_0{}^s$, $\theta_1{}^s$, $\tau_0{}^s$ and ($\tau_0{}^s + \tau_1{}^s$) are the slip system, initial and final slopes of the hardening curve, initial critical resolved shear stress, and the back-extrapolated CRSS, respectively. VPSC simulations begin with initial texture (~10,000 orientations) of AZ31-0.5Ca alloy that was used to predict the relative activities of slip systems during various stretching conditions. In this regard, CRSS and hardening parameters of each deformation mode were adjusted until the simulated textures matched with the experimentally received textures for all stretching conditions.

3. Results and Discussion

Figure 1 shows the microstructural features, texture and room temperature tensile properties of the AZ31-0.5Ca Mg alloy, investigated in the present work. It can be seen that this alloy has a fine-grained structure with weak basal texture, and interestingly, some twin boundaries (~4%) were observed in this alloy (tension twins at 86° as shown by Figure 1c). In addition, Figure 1d shows that this alloy exhibited an improved tensile ductility, which was higher than that of conventional AZ31 alloy. The enhanced ductility of the alloy is mainly related to the Ca addition and the intermetallic compounds (IMCs) that formed as a result of this addition. The EPMA maps of the alloy presented in Figure 1e confirmed the formation of the IMCs in the form of particles (~1 μm) and those particles are composed of Mg, Al and Ca, as shown by the EPMA maps associated with these elements.

For a further understanding on how such addition can contribute to the plasticity of the Mg alloy, EBSD observations were carried out on alloy samples stretched at various strains (5%, 10%, and 15%) and the counterpart VPSC calculations were then conducted. Figure 2 shows the inverse pole figure (IPF) maps of strained samples and the related microstructural and textural features. It can be noted that the straining of the alloy samples mainly lead to a further weakening in the basal texture, where most of orientations were tilted away from the normal direction pole and distributed along the rolling direction and this effect became more significant by increasing the amount of strain from

5% to 15% [11]. The grain size was also influenced by the magnitude of stretching where, after 15%, the structure was slightly coarser as compared to those after 5% and 10%; this is shown by arrows in Figure 2b. A more important trend was noticed from the misorientation angle distribution of the strained alloy samples, as shown in Figure 3c. In this trend, it can be noted that the fraction of the tension twin boundaries (at 86°) was higher as compared to that of the non-strained sample (Figure 1c) and this fraction decreased by increasing the magnitude of stretching, where fractions of 10%, 8% and 6% were observed in the samples strained at 5%, 10% and 15%, respectively. Even in such behavior, one can suggest the contribution of twins as a support mechanism to enhance the plasticity of this alloy; however, the fraction of the twins evolved in this alloy upon the stretching is still much smaller than that observed in conventional Mg alloy (~40% after 10% deformation) [12,13]. The lower activity of twin mode in this alloy can be attributed to the contribution of the more non-basal slip systems in the plasticity process. This can be roughly explored through the evolution of a larger fraction of low-angle grain boundaries (LAGBs) (<15%), where fractions of LAGBs of 30%, 40% and 55% were evolved in the samples strained at 5%, 10% and 15%, respectively. It is well known that boundaries with a low angle of misorientation—less than 15°—are considered as arrays of parallel dislocation lines. The higher activity of non-basal slip systems expected in this alloy based on the EBSD measurements is mainly attributed to the effect of Ca addition, which can be clarified through the VPSC calculations under the same stretching conditions. As aforementioned, initial orientations (~10,000 orientations) from the AZ31-0.5Ca alloy were introduced into the VPSC model, which were used to simulate the final textures received after the various pre-stretching conditions (5%, 10%, 15%). For each pre-stretching condition, the latent and voce hardening parameters were adjusted until the simulated pole figures (PFs) were almost identical to the experimentally obtained PFs. Figure 3 shows the simulated and received (0001) PFs for 5%, 10% and 15% stretched samples. It can be seen that VPSC modeling reproduced the PFs for all the various conditions successfully, indicating that the parameters used for conducting simulations are reliable. The CRSS values for various deformation modes for all the stretched conditions (5%, 10%, 15%) are listed in Table 1. The received values were found to be higher as compared to a Mg single crystal. It can be attributed to the formation of $(Mg,Al)_2Ca$ intermetallic particles as a result of Ca addition to AZ31 which, in turn, can act as an obstacle to plastic deformation. In addition, higher CRSS values of pyramidal slip were recorded for all the stretched conditions. However, some interesting differences in the CRSS of other deformation modes can be noticed. For instance, the CRSS of basal slip was received to be almost double to prismatic slip (50 vs 95) for the 5% stretched sample, while on the other hand, a smaller difference in CRSS of the basal slip and prismatic slip (57 vs 91) was observed for the 10% stretched sample. This difference was received to be further reduced as a result of 15% stretching (Figure 3b). It is already established that as the ratio ($CRSS_{Prismatic}/CRSS_{Basal}$) is reduced, it can lead to the higher activity of prismatic slip system which, in turn, can enhance the performance of the Mg alloy [14–17]. Figure 3c demonstrates the activities of prismatic slip, basal slip and tension twins in AZ31-0.5Ca, which was stretched by 15%, along the rolling direction. As is evident from Figure 3c, at the beginning of the deformation process, the basal slip acted as the dominating slip system. As the deformation process continued, higher activity of the prismatic slip was noticed, which eventually surpassed the basal slip for higher stretching conditions. In addition, a very low activity of tension twins was recorded during the deformation process.

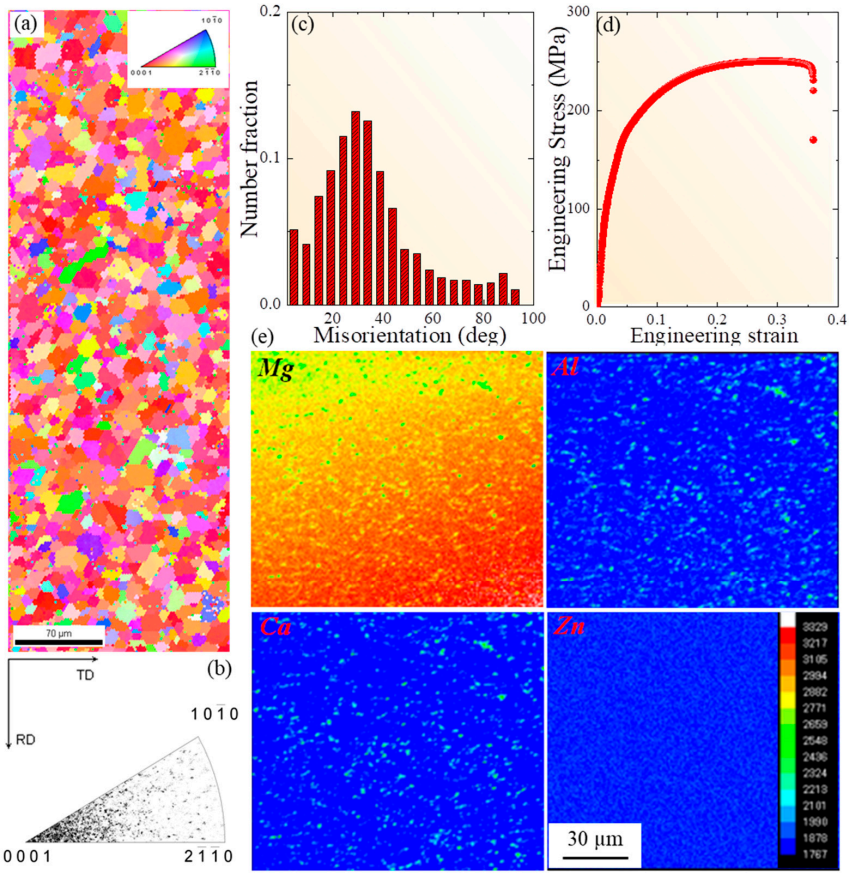

Figure 1. (**a**), (**b**) and (**c**) Inverse pole figure map, texture inverse pole figure, and misorientation angle distribution of the AZ31-Ca Mg alloy, respectively. (**d**) Room temperature tensile curve of the alloy. (**e**) Electron probe microanalysis maps of the alloy.

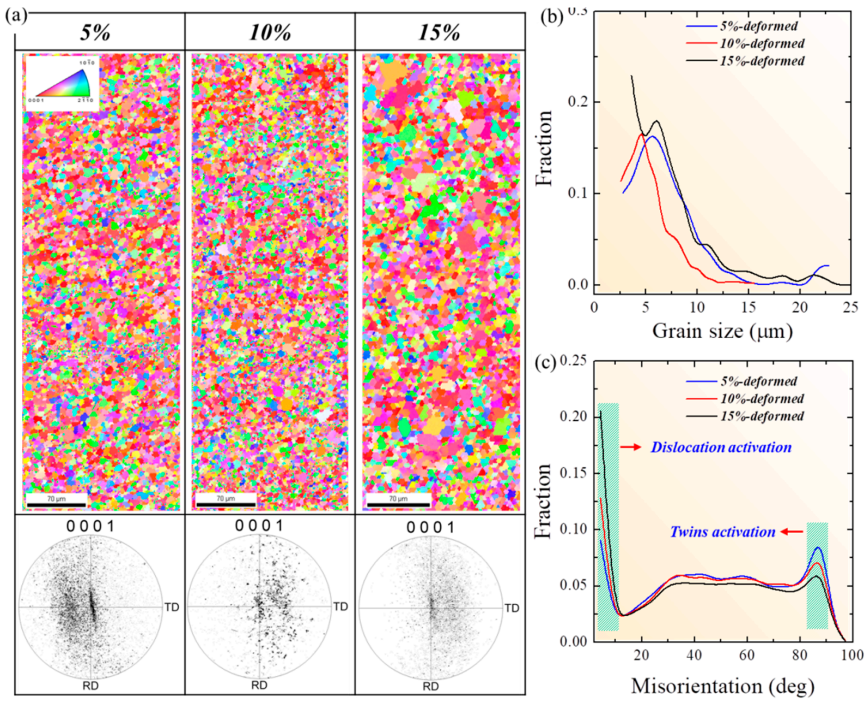

Figure 2. (**a**) Inverse pole figure maps and related 0001 pole figures of the AZ31-Ca Mg alloy samples stretched to 5%, 10% and 15%. (**b**) and (**c**) grain size and misorientation profile of the stretched alloy samples, respectively.

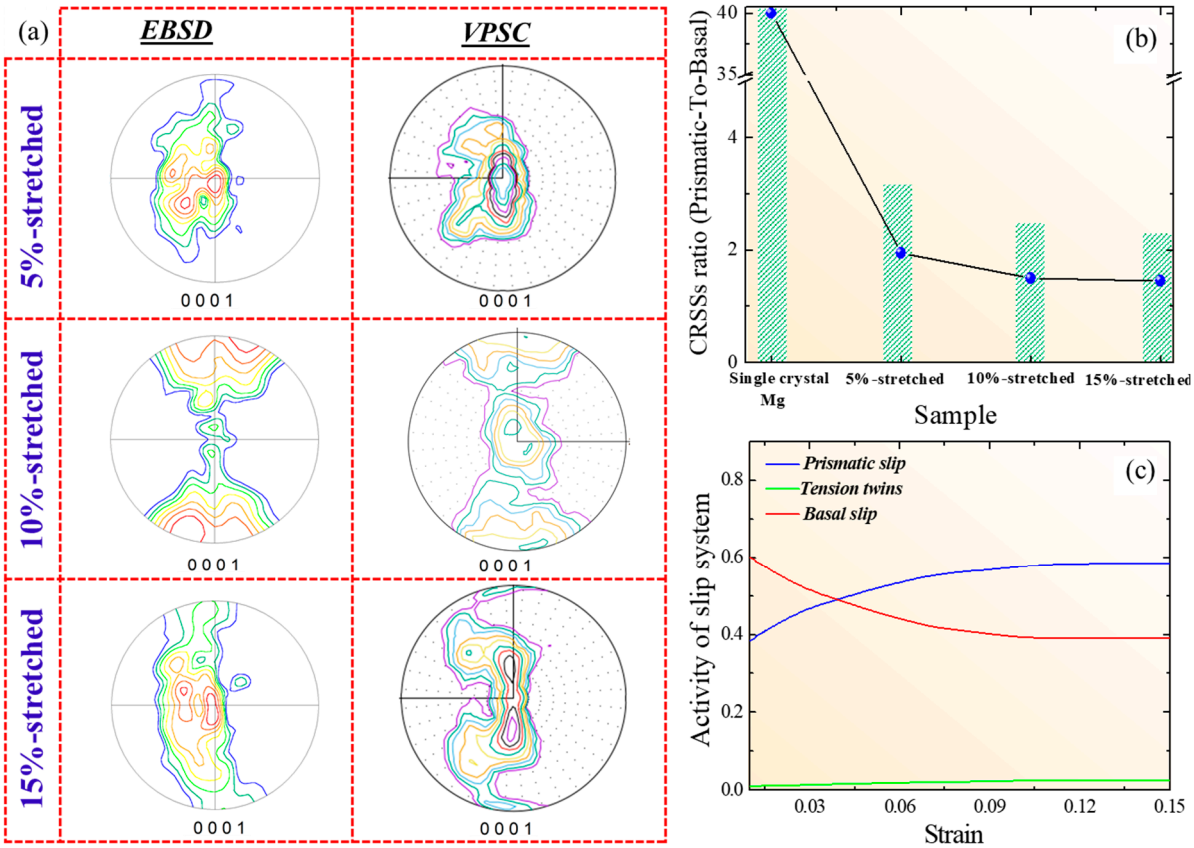

Figure 3. (**a**) Pole figures of the stretched samples obtained by the EBSD measurements and by VPSC modeling. (**b**) CRSSs ratio (prismatic/basal) of single crystal Mg and the stretched samples. (**c**) The activity of basal slip, prismatic slip and tension twins of the AZ31-Ca alloy investigated in the present work.

Table 1. CRSS values and hardening parameters for VPSC modeling of the samples (5%, 10%, 15% stretched).

Alloy Sample	Deformation Mode	τ_0	τ_1	θ_0	θ_1	$CRSS_P/CRSS_B$
5%	*<a> basal slip*	50	12	99	55	1.90
	<a> prismatic slip	95	29	135	10	
	<a + c> pyramidal slip	315	38	57	19	
	Tension twin	14	170	105	50	
10%	*<a> basal slip*	57	9	115	62	1.50
	<a> prismatic slip	91	37	148	8	
	<a + c> pyramidal slip	305	44	64	22	
	Tension twin	15	185	110	55	
15%	*<a> basal slip*	65	15	125	45	1.47
	<a> prismatic slip	96	35	137	9	
	<a + c> pyramidal slip	302	195	58	33	
	Tension twin	20	178	112	58	

In-crystal misorientation axis (ICMA) measurement carried out by EBSD is a useful tool to determine the type of slip system which might operate during deformation of metallic materials [18,19].

Generally, dislocations generated during the early stage of plastic deformation bend the crystal, leading to the so-called in-crystal misorientation, and through the characteristics of this misorientation axis, the type of dislocation can be determined. For example, basal dislocations induce the crystal bending around $\langle 10\bar{1}0 \rangle$, whereas an axis parallel to ⟨0001⟩ is obtained in the case of prismatic dislocation-plasticized crystals [20,21]. The ICMA measurements carried out on the stretched alloys samples are shown in Figure 4. The ICMA was conducted on three randomly selected grains from each sample. Figure 4 shows that the number of misorientation axes that come to be parallel with ⟨0001⟩ increased upon increasing the magnitude of stretching, suggesting that the crystal plasticity of this alloy is mainly aided by the prismatic dislocations rather than the activation of tension twins. This is consistent with the misorientation angle distributions and VPSC calculations presented in Figures 2c and 3, respectively. The higher activity of prismatic slip systems is mainly related to the Ca addition, which led to the formation of $(Mg,Al)_2Ca$ particles, as shown by the EPMA maps in Figure 1e. During the primary processing of the Ca-added Mg alloy, these particles can weaken the basal texture through inducing the recrystallization [22,23]. Accordingly, one way to explain the high activity of the prismatic slip is the particle-induced basal texture weakening, where in such a texture, a higher amount of stress can be resolved in the prismatic plane when comparing with strong basal-textured Mg, leading to the high activity of the prismatic slip. Another approach to figure out such high activity of prismatic slip is related to the strengthening effect of these particles in the basal plane which, in turn, lead to reducing the ratio between the CRSS of prismatic and CRSS of basal (Table 1). The intrinsically hard-to-operate prismatic slip becomes preferred relative to the extrinsically hardened basal slip, leading to the enhanced plasticity of the alloy investigated in the present work. Further transmission electron microscopy-based observations are required to investigate the nature and characteristics of the interaction between basal dislocations and particles in the AZ31- 0.5Ca Mg alloy.

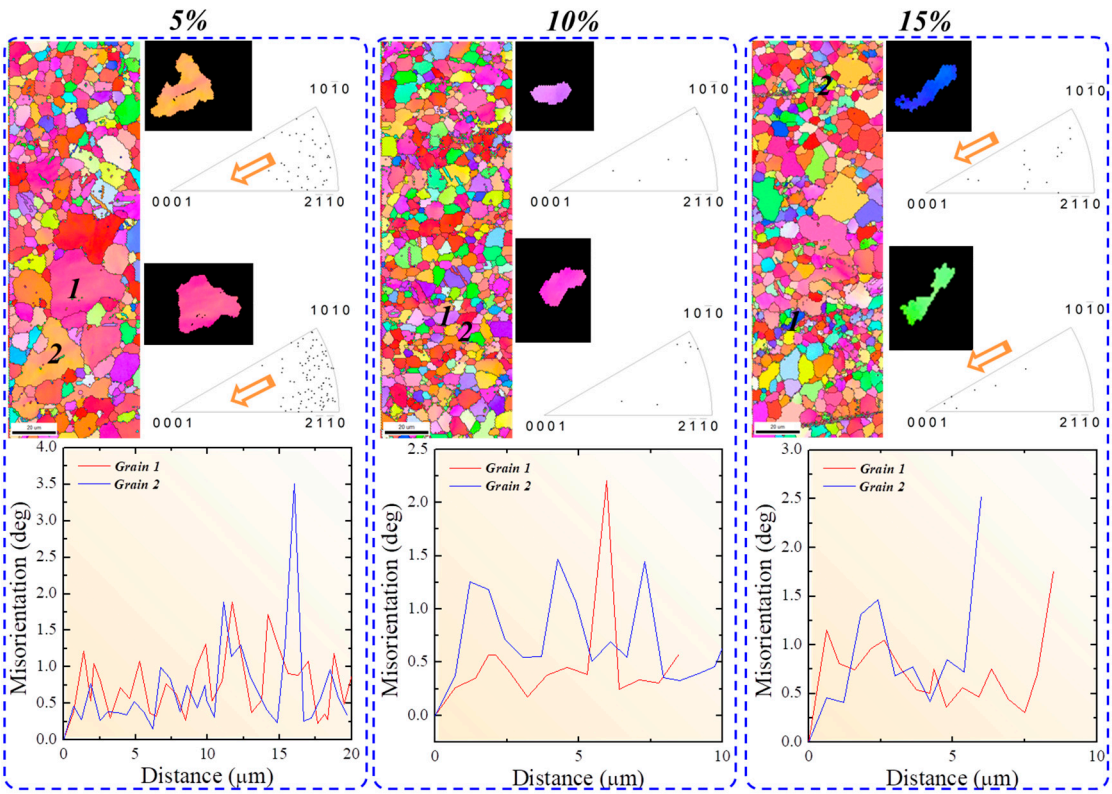

Figure 4. In-crystal misorientation axis (ICMA) measurements of the stretched samples. The misorientation profiles presented in this figure were taken from the grains used for the ICMA measurements.

4. Conclusions

In the present work, EBSD measurements supported by VPSC calculations were used to explain the high plasticity recorded in AZ31-0.5Ca alloys. The results showed that the plastic deformation in the alloy is mainly aided by the operation of dislocations rather than the activation of twinning. This is related to the texture weakening induced by the intermetallic particles formed in the AZ31 alloy due to the Ca addition. The strengthening effect of these particles on the basal dislocations, additionally, reduced the ratio $CRSS_P/CRSS_B$, leading to the higher contribution of prismatic slip in the plasticity of this alloy.

Author Contributions: K.H. and J.-G.K designed the experiments. U.M.C. carried out the experiments and VPSC simulations. K.H. and U.M.C. analyzed the data and wrote the manuscript. K.H., J.-G.K. and U.M.C. revised the manuscript. All authors have read and agreed to the published version of the manuscript.

Funding: This research was funded by National Research Foundation (NRF) of South Korea (2017R1C1B5017204).

Acknowledgments: The authors express their gratitude to ***C. N. Tomé*** (Material Science and Technology Division, Los Alamos National Laboratory) for providing the VPSC software to conduct the simulations. This research was supported by National Research Foundation (NRF) of Korea (2017R1C1B5017204).

Conflicts of Interest: The authors declare no conflict of interest.

References

1. Miller, V.M.; Berman, T.D.; Beyerlein, I.; Jones, J.W.; Pollock, T.M. Prediction of the plastic anisotropy of magnesium alloys with synthetic textures and implications for the effect of texture on formability. *Mater. Sci. Eng. A* **2016**, *675*, 345–360. [CrossRef]
2. Chaudry, U.M.; Hamad, K.; Kim, J.G. On the ductility of magnesium based materials: A mini review. *J. Alloys Compd.* **2019**, *792*, 652–664. [CrossRef]
3. Agnew, S.R.; Duygulu, O. Plastic anisotropy and the role of non-basal slip in magnesium alloy AZ31B. *Int. J. Plast.* **2005**, *21*, 1161–1193. [CrossRef]
4. Luo, D.; Luo, D.; Wang, H.; Zhao, L.; Wang, C.; Liu, G.; Liu, Y.; Jiang, Q. Effect of differential speed rolling on the room and elevated temperature tensile properties of rolled AZ31 Mg alloy sheets. *Mater. Charac.* **2017**, *124*, 223–228. [CrossRef]
5. Hamad, K.; Ko, Y.G. A cross-shear deformation for optimizing the strength and ductility of AZ31 magnesium alloys. *Sci. Rep.* **2016**, *6*, 1–8. [CrossRef] [PubMed]
6. Samman, T.Al.; Li, X. Sheet texture modification in magnesium-based alloys by selective rare earth alloying. *Mater. Sci. Eng. A* **2011**, *528*, 3809–3822. [CrossRef]
7. Sandlobes, S.; Pie, Z.; Friak, M.; Zhu, L.F.; Wang, F.; Zaefferer, S.; Raabe, D.; Neugebauer, J. Ductility improvement of Mg alloys by solid solution: Ab initio modeling, synthesis and mechanical properties. *Acta. Mater.* **2014**, *70*, 92–104. [CrossRef]
8. Chaudry, U.M.; Kim, T.H.; Park, S.D.; Kim, Y.S.; Hamad, K.; Kim, J.G. On the high formability of AZ31-0.5Ca magnesium alloy. *Materials.* **2018**, *11*, 1–15.
9. Agnew, S.R.; Yoo, M.H.; Tomé, C.N. Application of texture simulation to understanding mechanical behavior of Mg and solid solution alloys containing Li or Y. *Acta. Mater.* **2001**, *49*, 4277–4289. [CrossRef]
10. Lebensohn, R.A.; Tomé, C.N. A self-consistent anisotropic approach for the simulation of plastic deformation and texture development of polycrystals: Application to zirconium alloys. *Acta. Metal et Mater.* **1993**, *41*, 2611–2624. [CrossRef]
11. Khan, A.S.; Pandey, A.; Herold, T.G.; Mishra, R.K. Mechanical response and texture evolution of AZ31 alloy at large strains for different strain rates and temperatures. *Int. J. Plast.* **2011**, *27*, 688–706. [CrossRef]
12. Sandlobes, S.; Friak, M.; Kerzel, S.K.; Pie, Z.; Neugebauer, J.; Raabe, D. A rare-earth free magnesium alloy with improved intrinsic ductility. *Sci. Rep.* **2017**, *7*, 1–8. [CrossRef] [PubMed]
13. He, J.; Jiang, B.; Yang, Q.; Li, X.; Xia, X.; Pan, F. Influence of pre-hardening on microstructure evolution and mechanical behavior of AZ31 magnesium alloy sheet. *J. Alloys Compd.* **2015**, *621*, 301–306. [CrossRef]

14. Martin, R.S.; Prado, M.T.P.; Segurado, J.; Bohlen, J.; Urrutia, I.G.; Llorca, J.; Aldareguia, J.M.M. Measuring the critical resolved shear stress in Mg alloys by instrumented nanoindentation. *Acta. Mater.* **2014**, *71*, 283–292. [CrossRef]
15. Manrique, H.P.; Yi, S.B.; Bohlen, J.; Letzig, D.; Perez, P.M.T. Effect of Nd additions on extrusion texture development and slip activity in a Mg-Mn alloy. *Metall. Mater. Trans. A* **2013**, *44*, 4819–4829. [CrossRef]
16. Chaudry, U.M.; Kim, T.H.; Park, S.D.; Kim, Y.S.; Hamad, K.; Kim, J.G. Effect of calcium on the activity of slip systems in AZ31 magnesium alloy. *Mater. Sci. Eng. A* **2019**, *739*, 289–294. [CrossRef]
17. Angew, S.R.; Tome, C.N.; Brown, D.W.; Holden, T.M.; Vogel, S.C. Study of slip mechanisms in a magnesium alloy by neutron diffraction and modeling. *Scripta. Mater.* **2003**, *48*, 1003–1008.
18. Suh, B.C.; Kim, J.H.; Bae, J.H.; Hwang, J.H.; Shim, M.S.; Kim, N.J. Effect of Sn addition on the microstructure and deformation behavior of Mg-3Al alloy. *Acta. Mater.* **2017**, *124*, 268–279. [CrossRef]
19. Chun, Y.B.; Battaini, M.; Davies, C.H.J.; Hwang, S.K. Distribution characteristics of in-grain misorientation axes in cold-rolled commercially pure titanium and their correlation with active slip modes. *Metall. Mater. Trans. A* **2010**, *41*, 3473–3487. [CrossRef]
20. Chaudry, U.M.; Kim, Y.S.; Hamad, K. Effect of Ca addition on the room-temperature formability of AZ31 magnesium alloy. *Mater. Lett.* **2019**, *238*, 305–308. [CrossRef]
21. Yuasa, M.; Miyazawa, N.; Hayashi, M.; Mabuchi, M.; Chino, Y. Effects of group II elements on the cold stretch formability of Mg-Zn alloys. *Acta. Mater.* **2015**, *83*, 294–303. [CrossRef]
22. Trang, T.T.T.; Zhang, J.H.; Kim, J.H.; Zargaran, A.; Hwang, J.H.; Suh, B.C.; Kim, N.J. Designing a magnesium alloy with high strength and high formability. *Nat. Comm.* **2018**, *9*, 1–6. [CrossRef] [PubMed]
23. Kim, J.H.; Kang, N.E.; Yim, C.D.; Kim, B.K. Effect of calcium content on the microstructural evolution and mechanical properties of wrought Mg-3Al-1Zn alloy. *Mater. Sci. Eng. A* **2009**, *525*, 18–29. [CrossRef]